Numerical analysis on seismic resistance of a two-story timber-framed structure with stone and earth infill

E. Fritsch[a,b,d], Y. Sieffert [a,b], H. Algusab[a,b], S. Grange [e], P. Garnier[c], and L. Daudeville[a,b]

[a]Université Grenoble Alpes, 3SR, Grenoble, France; [b]CNRS, 3SR, Grenoble, France; [c]National School of Architecture of Grenoble, AE&CC Research Unit, CRAterre, Grenoble, France; [d]Faculty of Civil Engineering, Technische Universität Dresden, Dresden, Germany; [e]University of Lyon, INSA-Lyon, SMS-ID, Villeurbanne cedex, France

ABSTRACT

Due to their seismic resistance, traditional timber-framed structures with masonry infill suffered little damage during recent earthquakes. Moreover, timber-framed structures can be built with reduced costs thanks to the use of locally available materials such as wood, stone, and earth. Based on an experimentally validated numerical simulation for a one-story house, the seismic resistance of a similar two-story house is investigated. A simplified Finite Element Model with linear and nonlinear truss elements is proposed to analyze the seismic resistance of a two-story building. Nonlinear hysteresis constitutive laws are defined only for two majorcomponents of the structure which are assumed to be representative of the global structure behavior: diagonal X-crosses (concentrating the interaction with the infill material) and steel strip connections. These kinds of structures have been overlooked due to a lack of knowledge of their potential behavior in seismic prone area and a lack of building codes and standards for their own design. To promote them, a failure criterion, that might easily be used in engineering studies, is required. This article proposes a simple criterion based on Eurocode 8 to quantify the seismic resistance of one- and two-story houses. The simulation shows that, even in case of high intensity ground motion, the two-story building should not be collapsed. This study may help at designing two-story timber-framed structures in seismic prone areas for (re)construction projects.

Introduction

Seismic resistance of traditional timber-framed structures

Traditional timber-framed structures with masonry infill can be found in many countries all over the world, numerous of them are built in seismic prone areas (Vieux-Champagne et al. 2014b):

- *Pombalino* in Portugal,
- *Maso* in Italy,
- *Dhajji dewari* in Pakistan,
- *Bagdadi* in Turkey,
- *Kay peyi* in Haiti,
- *Colombages* in France,
- *Fachwerk* in Germany,
- *Casa baraccata* in Italy,
- *Quincha* in Pero.

Traditional timber-framed buildings are known to be efficient earthquake resistant structures (Langenbach (2007), Dutu, Sakata, and Yamazaki 2014) and suffered little damage during recent seismic events. Timber-framed structures can be built with better economic efficiency thanks to the use of locally available materials such as wood, stone, and earth. These kinds of structures are also relevant for sustainable development and to cease wasting the precious natural resources which are available in limited quantity (Sieffert, Huygen, and Daudon 2014). In Haiti, multiple timber-framed structures are built within various reconstruction projects (Joffroy et al. 2014). The selected house is prevalent in Haitian timber-framed reconstruction programs initiated after the 2010 earthquake; it provides an enhancement over traditional buildings by improving the connection of the timber structure with both the basement and foundation, and by introducing bracing via San Andrew's crosses (X-cross) filled with natural stones and bonded by earth mortar using sisal, as shown in Figure 1. To enhance the knowledge about the seismic resistant behavior of traditional timber-framed structures, experimental and numerical investigations were conducted (Ruggieri, Tampone, and Zinno 2015). Focusing on ongoing reconstruction projects in Haiti, the seismic resistance of a one-

CONTACT Y. Sieffert yannick.sieffert@3sr-grenoble.fr Universite Grenoble Alpes, Saint-Martin-d'Heres, 38402 France.



(a) Traditional house built in Haiti (Photograph: F. Vieux-Champagne, 2010, Cap Rouge, Haiti)



(b) Recent house built in the reconstruction project (Photograph: Elsa Cauderay, n.d., Terre rouge Petit Goâve, Haiti)

Figure 1. Rural haitian houses.

story house was analyzed with a multiscale approach. Quasi-static tests performed on joints, elementary cells, and shear walls were used to calibrate the numerical model used for the one-story traditional timber-framed house (Vieux-Champagne et al. 2014b). Seismic tests performed on a full scale wall and one-story house were used to validate the model (Sieffert et al. 2016, Vieux-Champagne et al. 2017).

One-story timber constructions are often used for residential houses, whereas two-story constructions are also suitable for school buildings or hospitals. Figure 2 shows a two-timber-framed school recently built in Grand Boulage. For these buildings, a good earthquake resistance is required but actually no experimental or numerical analysis was carried out to assess their seismic performance. Based on the detailed numerical investigation on both a shear wall (2D) and a one-story house (3D) by Vieux-Champagne et al. (2017) and Vieux-Champagne et al. (2014a), a similar analysis is conducted on a two-story house (3D) under seismic loading by using the parameters identified in the previous work. Then the proposed article consists in the first analysis of the seismic performance of a two-story traditional building with stone and earth infill. This is not a specific case study



Figure 2. Two-story timber-framed house in Grand Boulage (Courtsey of the NGO Entrepreneurs du Monde).

but it is inspired from a recent construction a school house in Grand Boulage. This study is based on a previous work performed on a one-story building (Sieffert et al. 2016, Vieux-Champagne et al. 2017).

The two-story timber-framed house

A typical two-story traditional timber-framed structure is shown in Figure 2 and the timber frame is schematized in Figure 3. The construction details were choen by architects of the National School of Architecture at Grenoble involved in technical support for NGOs in Haiti.

At the bottom, a sill plate is fixed to the foundation (masonry wall). In this study, similarly to previous work (Vieux-Champagne et al. 2017), the soil-structure interaction is not considered; the numerical model doesn't include the foundation and its connection to the wooden structure. As illustrated in Figure 6, the posts are connected to this beam with a steel strip which clasps the beam and which is then fixed to the post with eight nails (3 mm × 70 mm).

The walls consist of posts connected by diagonal St. Andrew's crosses and noggins. The St. Andrew's crosses and the noggins are fixed with nailed connections to the posts (Figure 7). The space between the framework is filled up with masonry consisting of limestones, earth mortar, and sisal fibres. Onto the inner parts of the framework, nails are used to increase the grip between the wooden trusses and the infill in order to limit the risk of drop-out of the infill.

Between the first and the second story, a top plate separates the posts of the first and second story. The lower and upper parts of the posts and the top plate are connected at both sides of the wall thanks to steel strips similar to the ones used to connect the posts and the sill plate (Figure 8b). At the corners, steel strips are used on each face (Figure 3).

The main girders consist each of two parallel beams which are attached to the lower posts with six bolts. For this connection, a sufficient width of the post (20 cm) is required to avoid short distances from the bolts to the outline of the posts. As a consequence, the width of 10 cm chosen for the one-story house is not sufficient and therefore modified to 20 cm for the two-story house. The connection is shown in Figure 8a. As the girders are only attached in one main load bearing direction, only the two connected walls are modified for the above-mentioned constructional reasons. It is supposed that the enlargement does not reduce neither the vertical or horizontal load capacity of the post nor the load capacity of the metal connection. Rather, an increase of the load capacity can be estimated. Therefore, a conservative approach is used for the simulation: the width of all posts is set at 10 cm to simplify the modeling.

Orthogonal to the girders, beams are put at a distance of 0.45 m. For fire protection and sound insulation, a gypsum plasterboard and a 15-cm thick layer of light hemp concrete is optional. Onto this, wooden boards are used as floor. Theses wooden boards are taken into account for deadload but not as a structural floor bracing the structure in plane (XoY).

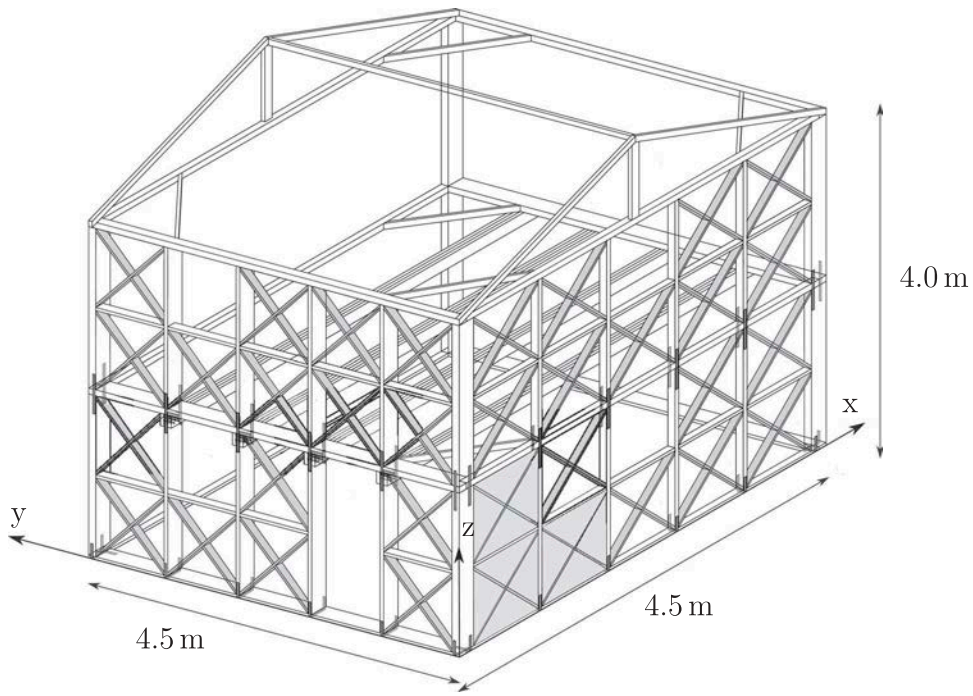


Figure 3. Structure for a two-story house.

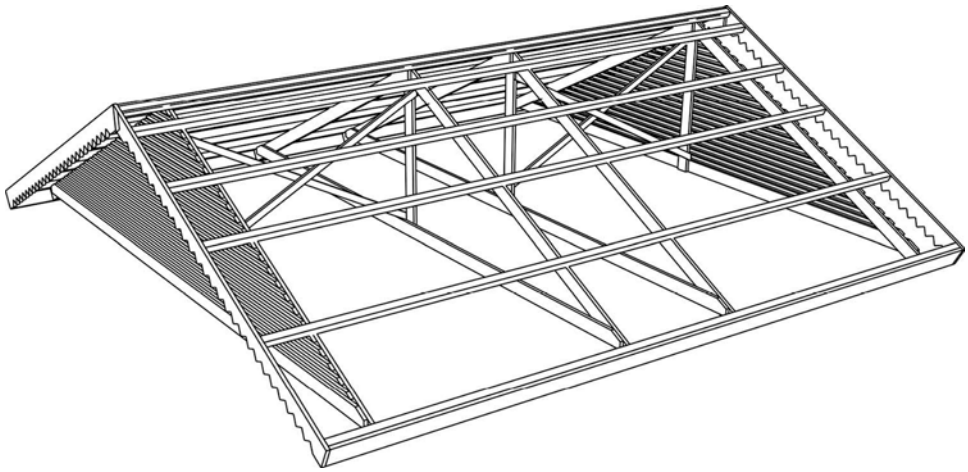


Figure 4. Roof truss dimensions (sketched by C. Belinga Nko'o).

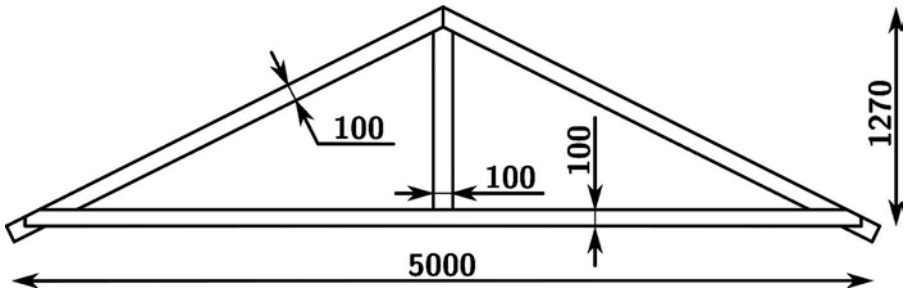


Figure 5. King post truss dimensions.

The roof is a lightweight wooden structure with roof trusses parallel to the girders of the floor. In longitudinal direction, the roof is braced with diagonal trusses. The detailed stiffening elements of the roof are not shown in Figure 3 but are presented in Figures 4 and 5.

An essential element for the resistance against horizontal forces are the horizontal, diagonal braces in the corners of the house.

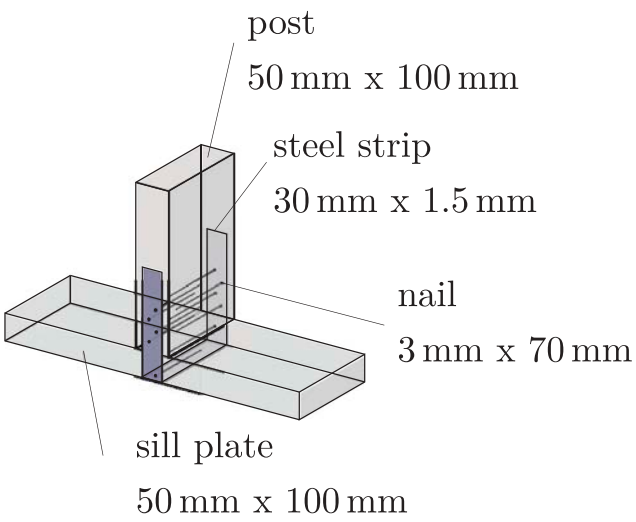


Figure 6. Connection of a post to the sill plate.

Modeling of the structure

Concentrating non linear phenomena in joints for studying the response of modern timber-framed structures under quasi-static or dynamical load is very classical

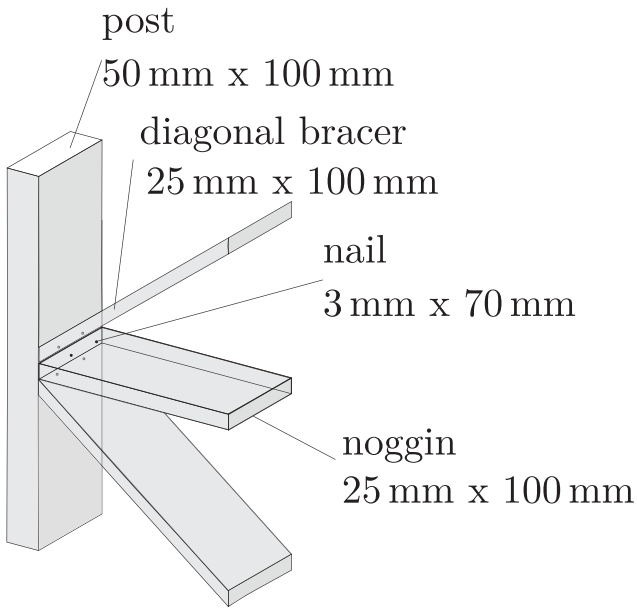
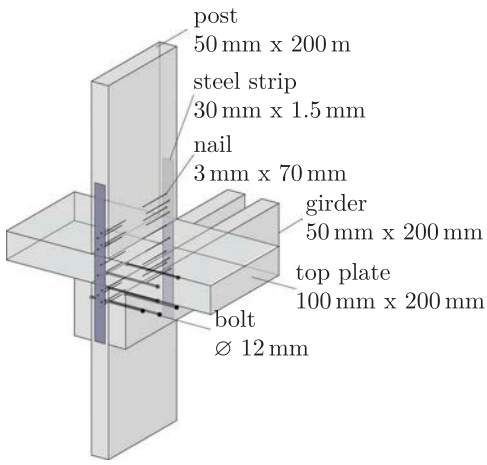
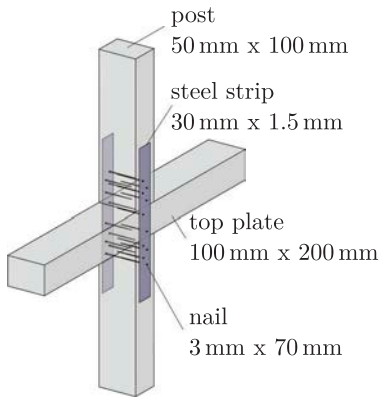


Figure 7. Connection of post, diagonal X-crosses, and horizontal plank.



(a) walls connected to the girders of the slab



(b) walls parallel to the girders of the slab

Figure 8. Connections of posts and top plates.

(see Dolan 1989, White and Dolan 1995, Kasal, Leichti, and Itani 1994, Humbert et al. 2014, Boudaud et al. 2015) since dowel-type joints are generally used. In the present study, dissipative phenomena are due to yielding in joints but also to complex phenomena (cracking, friction) occurring in the earth infill. So, two kind of nonlinear elements were used, first the joint elements for steel strip connections and second the X-crosses for both damage in the infill and the nailed connections with the frame.

Finite elements and constitutive behavior

The simulations have been performed using finite element code **ATLAS** developed with Matlab (Grange 2016). In the simulation, both the timber-framed structure and the infill are represented by a lattice-type structure with linear and non-linear truss elements, as it is shown in Figure 9. Finally, the house is modeled with 418 elements and 734 degrees of freedom. Timber frame parameters are given in section D. (D.1 and D.2) and nonlinear structural elements are modeled by using linear beam elements whose parameters are given in Tables C.1 and C.2 and Figure 26. The posts and the top plate between the two stories are modeled by means of linear beam elements.

The description of the diagonal X-crosses requires nonlinear elements. This results to the following consequences: the friction between the infill and the wooden X-crosses are not separately taken into account but both included in the behavior of the diagonal X-crosses; the application to the resistance regarding the damage of the infill; and most of the nonlinear behavior is coming from the deformations in the nail connections at both ends of the diagonal X-crosses. Finally, all the nonlinearities are concentrated in the the diagonal element. The tension

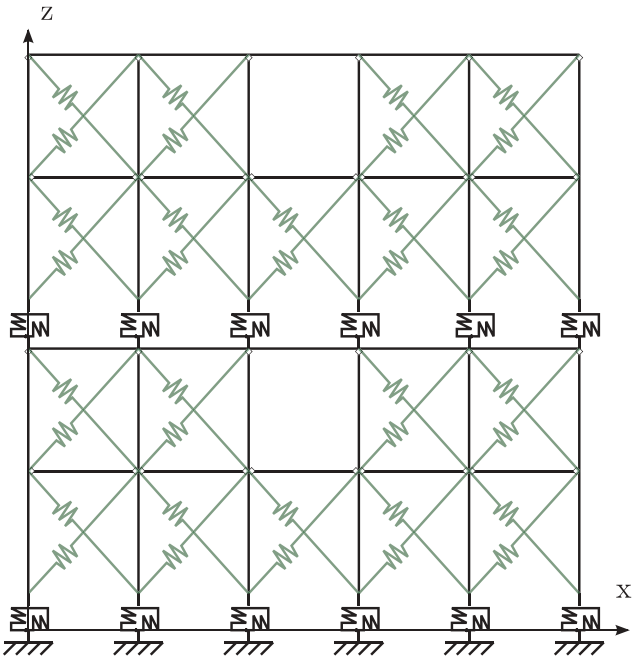


Figure 9. Lattice-type modeling of the wall with nonlinear elements.

and compression behaviors are different enabling accounting a possible unilateral contact (parameters are given in Tables C.1 and C.2). Then for large values of displacements, the joint becomes ineffective and the member could work only in compression.

The second type of non-linear element is the steel strip connection between the top plate and the posts. The resistance consists of a vertical (tension and compression) and a horizontal (shear) part. Both of them have been tested by Vieux-Champagne et al. (2014b) in an experimental setup consisting only of one horizontal beam and one post connected by the steel strip. Such a

modeling approach is classical for timber-framed structures (Andreasson, Yasumura, and Daudeville 2002, Yasumura et al. 2006, Richard et al. 2002, Xu and Dolan 2009). Both the nonlinearity in the diagonals and in the steel strip are described by a non linear constitutive law (Humbert et al. 2014). This model allows to describe the metallic timber-timber connection taking into account the damage under reverse loading, which means a strength reduction. Figure 10 shows the force-displacement curve that describes the constitutive behavior of the steel strip connection in tension and in shear for both a monotonic and reversed loading of the connection. Note that a similar constitutive behavior has been chosen to model the nonlinear diagonal element. The notation considers the asymmetric features: The superscript $+$ corresponds to the first direction of loading, the superscript $-$ refers to the opposite direction.

Branches ⓪ to ③ represent the monotonic loading. Starting linearly from zero to the yield displacement d_y with branch ⓪, the nonlinear phenomena in the joints are modeled by branch ① (rational quadratic Bézier curve) up to the force peak at (d_1, F_1). Finally, branches ② and ③ model with the same ponderation equal to 1.0 up to the failure of the joint at (d_u, F_u). The characteristic physical parameters (forces, displacements, stiffness) are shown in Table 1a.

The description of the cyclic group starts at (d_{pk}, F_{pk}), which corresponds to the value at the previous loop. After an elastic unloading (branch ④) down to a null force, a residual displacement d_c due to plastic deformations in the joint is observed. Finally, a loading into the opposite direction is described by branch ⑤. The shape of the hysteresis loop is controlled by parameters C_1 to C_4 (Table 1b) which are characteristic for each type of joint and loading direction. In Vieux-Champagne et al. (2014a), the curve is adapted to the nonlinear behavior of each the diagonals and the vertical and horizontal spring element for the shear wall connexions. For the simulation, the parameters for the diagonals are validated

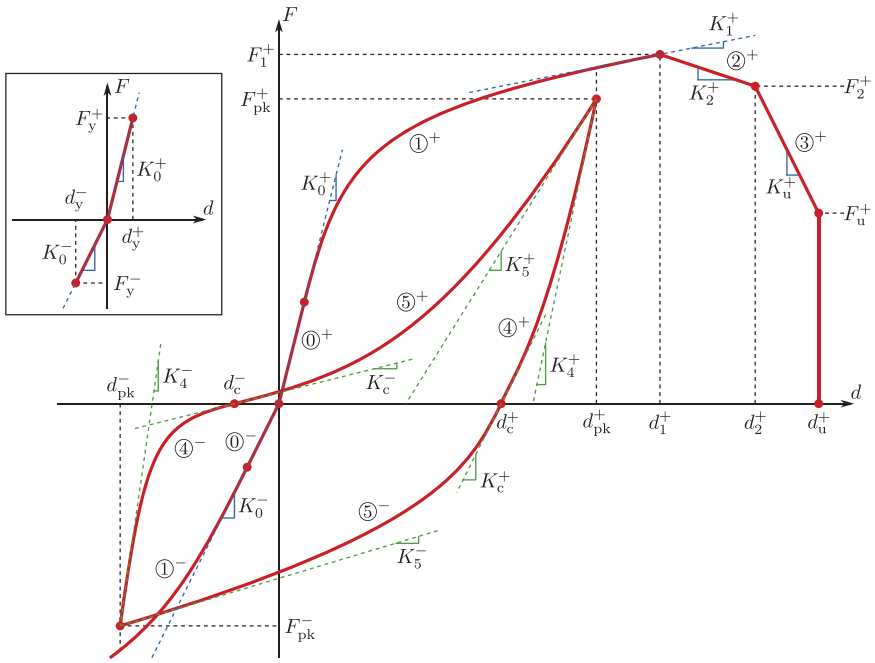


Figure 10. Force-displacement constitutive law (Courtesy of Humbert (2010)]).

Table 1. Model parameters.

(a) governing the behavior under monotonic loading		(b) governing the shape of hysteresis loops	
Parameter	Description	Parameter	Controls
d_y	Yield limit	C_1	Unloading stiffness
d_1	Displacement at peak force	C_2	Reloading stiffness
d_2	Intermediate displacement limit	C_3	Tangent stiffness at F = 0
d_u	Ultimate displacement	C_4	Residual displacement
F_1	Peak force		
F_2	Force at intermediate limit d_2		
F_u	Force at ultimate displacement d_u		
K_0	Initial elastic stiffness		
K_1	Pre-peak tangent stiffness		

with static experiments for a horizontally fixed shear wall. A curve for tension and one for compression is defined. For the vertical spring elements, the maximum force F_1 and the displacement d_1 is taken from the single steel strip connection tests. Again, two curves are characterized; one for tension and the other one for compression. For the horizontal support however, the shear resistance is symmetric. Since the horizontal spring elements have to take into account friction impacts, the horizontal support of the diagonals and the horizontal resistance of the steel strip, the value of its maximum force F_1 is increased. This value was identified by simulations of push over tests performed on shear walls (Vieux-Champagne 2013). After the calibration procedure, the parameters have been kept constant for all the other simulations. That is why the behavior of the one story building has been predicted in blind (Vieux-Champagne et al. 2014a). The parameters that have been chosen for the Humbert law are listed in Tables C.1 and C.2 for both the diagonals and the support elements.

To model the steel strip connection between the first and the second story (see Figures 8a and 8b), the same nonlinear element as for the steel strip connection at the bottom (see Figure 6) is used. This approximation is justified by the similarity of both connections, namely the same number of nails as well as the same type of steel strip.

Every opening in the wall such as doors and windows is created by removing the diagonal nonlinear elements in the respective cells. The floor structural system (Figure 11) is modeled with unidirectional elastic elements. The cross sections of these elements are given in Appendix D. Connections between the beam network (and equivalent concrete slab deadload) and posts are considered as rigid.

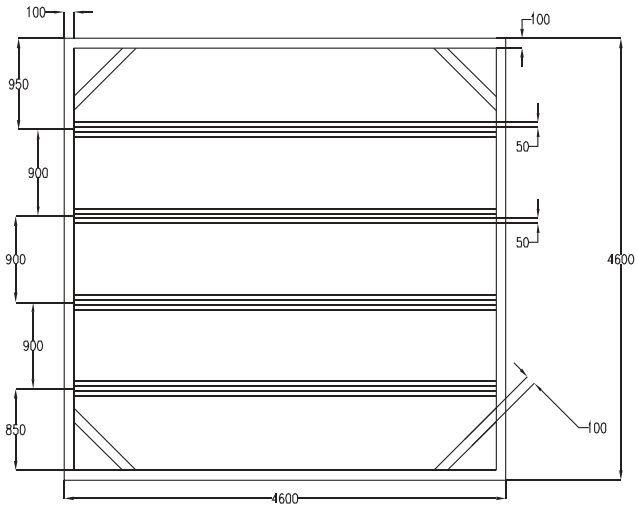


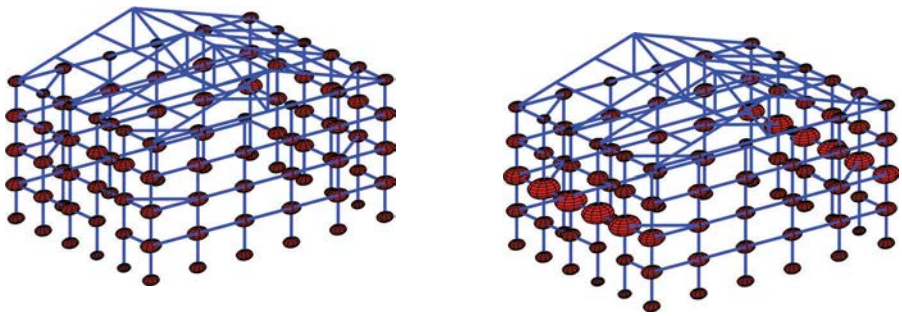
Figure 11. Top view of floor structural system.

Distribution of masses

As a FEM model is used, all masses are concentrated in element nodes.

Compared to the light wooden frame structure, the mass of the masonry infill predominates the total mass. The mass of one square element of masonry infill (0.9 m x 1.0 m) with a thickness of 6–10 cm is 150 kg (Vieux-Champagne et al. 2014b). This mass is evenly distributed to the four nodes of the respective square. Figure 12a shows the house with the masses of the walls concentrated to the element nodes. The volume of a sphere is equivalent to the mass at the node. Each two nodes which are connected by a steel strip (see Figure 9) have identical coordinates. Therefore, the masses of the two nodes are added and combined in one sphere for this figure. In the simulation, each of the two nodes connected by a steel strip has its own mass depending on adjacent filled squares.

For dynamical loading, the mass of the ceiling has a significant influence on the behavior of the house. As



(a) mass of masonry walls

(b) mass of masonry walls and concrete layer

Figure 12. Mass distributed to nodes.

mentioned above, a wooden support structure combined with gypsum plasterboard and a light hemp concrete infill is chosen. As calculated in Appendix A, the self-weight of the ceiling onto one girder is 61 kg. This additional mass is very small compared to the mass of the wall and can be therefore neglected. Instead, the influence of a heavier slab with a 7 cm concrete screed layer is simulated, which corresponds to a mass of 600 kg per girder. The mass of the ceiling is transferred to the lower posts by the four girders. Considering the mass of the ceiling, Figure 12b shows a significant increase of the masses.

Boundary conditions

Figure 13 gives an overview about the setting of the boundary conditions. The sill plate at the bottom of the house is considered as rigidly fixed to the soil (no soil structure interaction). As a consequence, it can be replaced by multiple single connection points to the vertical posts. At these points, all translatory movements and all rotations are set to zero. The bottom nodes of the wooden lattice structure are connected by steel strips to these points. The behavior of the steel strip is separated into a shear and a normal (vertical) force-slip relationship. Therefore, a relative displacement between the fixed points of the sill plate and the bottom nodes in horizontal and vertical direction is allowed (in the plane of the wall). The rotational resistance of the steel strip is neglected, the connected diagonals and vertical posts are then hinged to the bottom nodes and can rotate. A relative displacement between the fixed points and the bottom nodes in an orthogonal direction of the wall is impeded by the floor construction and the steel strip. A rotation around the horizontal axis of the plane is possible. In the corners, the boundary conditions for both shear walls are combined. As a consequence, the bottom nodes of corner posts are fixed in all horizontal directions.

For the nodes connected by the steel strips between the first and the second story, in general the same conditions are applied. However, as none of the nodes is fixed in any direction, only a relation between the nodes connected by a steel strip can be specified. The kinematic relationship orthogonal toward the wall is identical for two connected nodes between the steel strip, but for both, the vertical displacements are obtained by the shear constitutive law of the strip steel.

Dynamic loading and time integration

The dynamic inertial forces onto the nodes is calculated as function of the horizontal acceleration and the mass at each node. As acceleration, a synthetic signal of the Haiti earthquake from January 12, 2010 is used. As there was no recording station in Haiti, the signal was generated from other, less intense, recorded signals. A synthetic signal was developed using an approach which is described in Kohrs-Sansorny et al. (2005). This signal is denoted as the 100% signal for the simulation. For the test performed on a one-story house (Vieux-Champagne et al. 2017), this signal was transferred to the shaking table via a hydraulic system. Figure 14 shows the temporal course of the signal and the spectral acceleration. The maximum acceleration value is 2.7 m/s^2. To increase the impact on the house, the acceleration values are later multiplied by 2 (200%) or 3 (300%). In contrast to the experimental tests, in the simulation the 200% or the 300% loading is

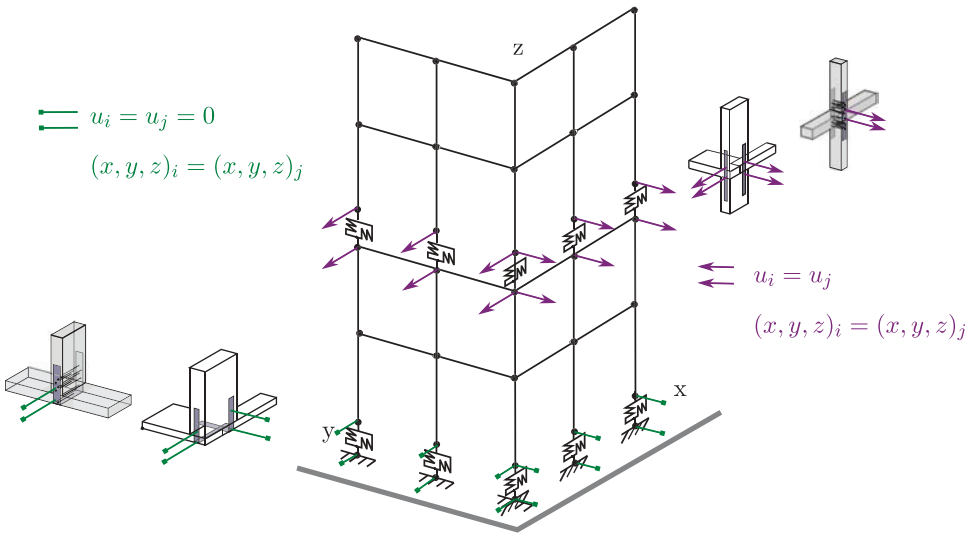
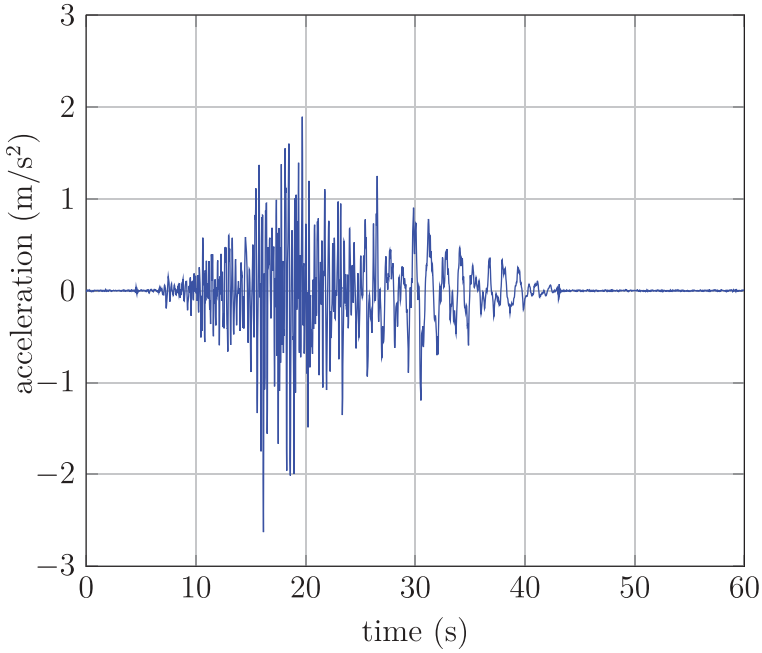
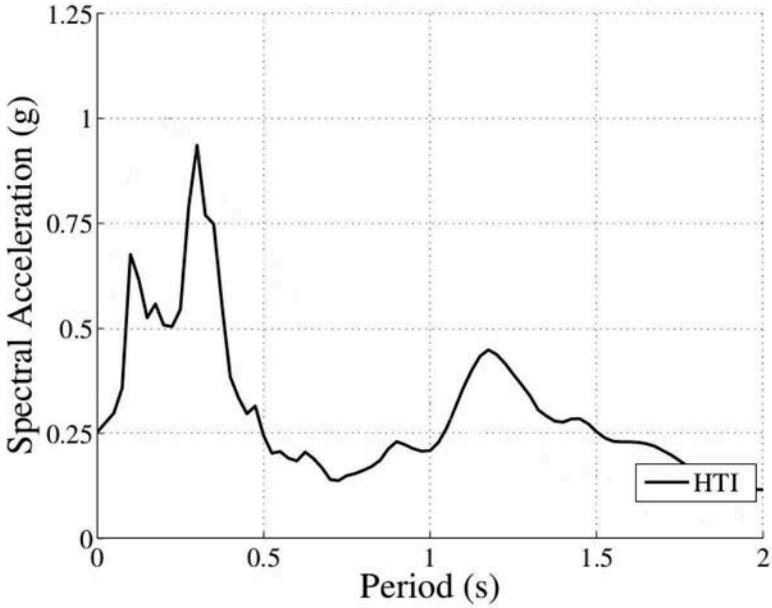


Figure 13. Boundary conditions.



(a) temporal signal



(b) spectral signal

Figure 14. 100 % signal Haiti January 12th.

applied to an intact house which has not experienced any loading before. For time discretisation, the Newmark method is used (Newmark 1959). To model viscous damping, the Rayleigh method is used. The damping matrix **C** is described with

$$\mathbf{C} = \alpha\mathbf{M} + \beta\mathbf{K}, \tag{1}$$

where **M** is the mass matrix, **K** is the stiffness matrix and the parameters, α and β depend on two natural frequencies ω_1 and ω_2 of the system as well as the damping ratio ξ:

$$\beta = \frac{2\xi}{\omega_1 + \omega_2} \tag{2}$$

$$\alpha = \omega_1\omega_2\beta. \tag{3}$$

The natural frequencies ω_1 and ω_2 are determined experimentally (see section B), as well as the damping ratio ξ from white noise tests at very low acceleration

amplitude in order to avoid damage. For the one-story house (Vieux-Champagne 2013), a 5% damping ratio was identified for a maximum acceleration of 0.3 m/s^2. Note that at higher accelerations, material dissipation may occur and the energy dissipation is mainly due to hysteretic phenomena in materials and joints. For that reason, it is assumed that viscous damping can be neglected and that nonlinear phenomena are only due to material hysteretic damping for the two-story house.

Results

Using the results of the numerical calculations, the impacts on the timber-framed house are compared concerning the following aspects:

- one-story vs. two-story house;
- direction of acceleration (x or y); and
- influence of the mass of the slab.

Table B.1 presents the natural frequencies obtained with the numerical model for the one and two-storey house. Table 2 gives an overview about the simulations which were run for the two-story house. To reference to an equivalent simulation for the one-story house, the index *-os* will be used. In the following discussion, *shear walls* and *front walls* will be differentiated. The walls parallel to the direction of acceleration are termed as *shear walls*; the walls which are orthogonal to the direction of acceleration are *front walls*.

Table 2. Simulations for the one-story and two-story house.

N°	Direction of acceleration [–]	Force of acceleration [%]	Mass of the slab [kg per beam]
1-os	y	100	-
1	y	100	-
1a	y	100	600
2-os	y	200	-
2	y	200	-
2a	y	200	600
3-os	y	300	-
3	y	300	-
3a	y	300	600
1x-os	x	100	-
1x	x	100	-
2x-os	x	200	-
2x	x	200	-
3x-os	x	300	-
3x	x	300	-

Displacements and forces

Figure 15 illustrates the decisive nodes for forces and displacements. For an acceleration in y-direction, the nodes represent:

ⓐ At this node, the tensile reaction force in vertical direction is maximal. The vertical displacement in the steel strip connection under tensile load is decisive for the resistance of the connection.

ⓑ and ⓒ

The maximum horizontal displacement in y-direction is measured. With this value, the drift of the shear wall can be calculated.

ⓓ and ⓔ

For the front wall, the total displacement orthogonal toward the wall is studied.

For an acceleration in x-direction, the nodes represent the following.

ⓗ At this node, the tensile reaction force in vertical direction is maximal. The vertical displacement in the steel strip connection under tensile load is decisive for the resistance of the connection.

ⓘ and ⓙ

The maximum horizontal displacement in x-direction is measured. With this values, the drift of the shear wall can be calculated.

ⓕ and ⓖ

the total displacement orthogonal toward the wall is studied.

The maximum displacements and forces at the decisive nodes for an acceleration in y-direction are shown in Table 3 and for an acceleration in x-direction are

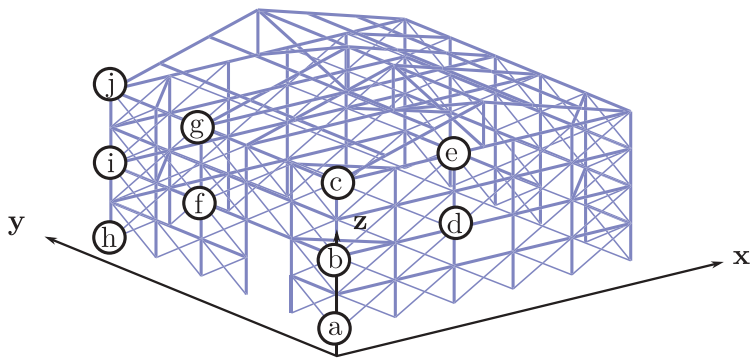


Figure 15. Nodes for force and displacement evaluation.

Table 3. Maximum values of forces and displacements for an acceleration in y-direction.

Simulation			1-os	1	1a	2-os	2	2a	3-os	3	3a
Time		[s]	16.68	19.80	19.80	18.46	19.80	19.83	18.44	19.80	16.52
ⓐ	F_{tens}	[KN]	1.90	2.67	4.53	2.77	6.29	6.15	3.61	7.11	7.50
	u_z	[mm]	0.25	1.11	1.47	0.62	3.19	3.03	0.90	4.63	4.83
	F_{tens} capacity ratio	[%]	17	24	41	25	57	56	33	65	68
	1-os ratio	[%]	100	140	238	146	331	324	190	374	395
ⓑ	u_y	[mm]	1.85	7.45	9.43	4.80	18.06	21.77	7.83	27.05	29.59
	drift shear wall	[%]	0.09	0.37	0.47	0.24	0.90	1.09	0.39	1.35	1.48
ⓒ	Δu_y	[mm]	-	2.26	2.64	-	5.20	5.30	-	7.50	7.15
	drift shear wall	[%]	-	0.11	0.13	-	0.26	0.26	-	0.37	0.36
ⓓ	u_y	[mm]	8.45	9.49	13.25	11.04	26.66	27.37	8.18	38.57	36.74
	drift front wall	[%]	0.04	0.47	0.66	0.55	1.33	1.37	0.41	1.93	1.84
ⓔ	Δu_y	[mm]	-	8.66	4.65	-	5.40	9.22	-	9.66	12.10
	drift front wall	[%]	-	0.43	0.23	-	0.27	0.46	-	0.48	0.60

Table 4. Maximum values of forces and displacements for an acceleration in x-direction.

Simulation			1x-os	1x	2x-os	2x	3x-os	3x
Time		[s]	18.81	16.46	18.48	19.76	19.75	18.57
ⓗ	F_{tens}	[KN]	1.08	3.63	2.07	5.40	3.60	7.30
	u_z	[mm]	0.16	0.91	0.44	2.26	1	4.66
	F_{tens} capacity ratio	[%]	10	33	19	49	33	67
	1x-os ratio	[%]	100	336	192	500	333	679
ⓘ	u_x	[mm]	1.53	4.13	4.20	9.60	6.25	17.98
	drift shear wall	[%]	0.08	0.21	0.21	0.48	0.31	0.90
ⓙ	Δu_x	[mm]	-	2.60	-	5.25	-	6.96
	drift shear wall	[%]	-	0.13	-	0.26	-	0.35
ⓕ	u_x	[mm]	6.61	13.24	7.13	16.12	14.70	40.00
	drift front wall	[%]	0.33	0.66	0.36	0.81	0.74	2.00
ⓖ	Δu_x	[mm]	-	0.15	-	3.76	-	−13.05
	drift front wall	[%]	-	0.01	-	0.19	-	−0.65

shown in Table 4. In these tables, the maximum values are noted when the node Ⓒ reaches is maximal value in the *y*-direction for the sollicitation in this direction and when the node ⓙ reaches its maximal value in the *x*-direction for the solicitation in this direction.

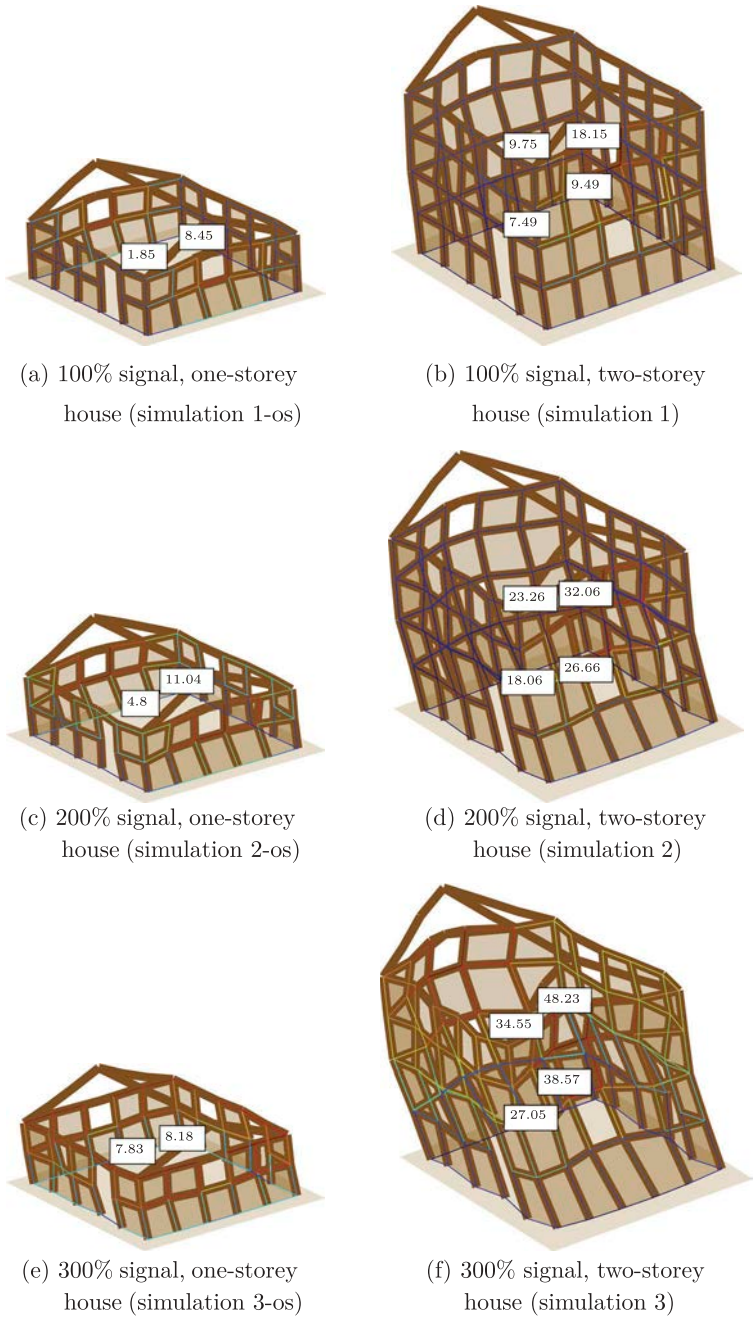
For the one-story house, the node ⓒ, ⓔ, ⓖ, and ⓙ do not exist.

Acceleration in *y*-direction

To compare the impact on the one-story house with the impact on the two-story house, the deformed structure during the loading is shown in Figure 16. In this first investigation, the slab mass is not considered. Deformed configurations are plotted when the maximum displacement of node ⓔ (in *y* direction) is reached. Due to the inertial forces of the second story, an additional force is exerted on the walls of the first story. Consequently, the displacements of the first story walls increase significantly for the two-story house. For the simulation with a 100% signal, the displacements increase fourfold for the shear wall (node ⓑ), whereas the displacements triple for the simulation with a 300% signal. The displacements in the middle of the front wall (node ⓓ) increase by the factor 1.1 for a 100% signal and by a factor 4.7 for a 300% signal. This indicates the rising impact in particular on the shear walls, which transmit the horizontal forces to the fixations at the bottom of the house. Moreover, the steel strip at the bottom (node ⓐ) is under twofold tensile load for the two-story house and 300% signal. This connection is stressed by the deformation of the shear wall, which tries to uplift its outer post.

Figure 18 compares the ridge displacement in *y*-direction near the strong phase (the part of the signal where the energy is maximum, i.e., the acceleration, the velocity, and the displacement are bigger simultaneously) of the three signals (between 16 s and 22 s) for one- and two-story. For the one-story building, the maximum positive displacement is, respectively, 9.35 mm, 16.91 mm, and 21.76 mm for 100%, 200%, and 300% signal, whereas it is respectively 19.44, 34.04, 50.40 mm for the two-story building. Then, the multiplying factor is similar for the one- (1, 1.8, 2.3) and two-story (1, 1.8, 2.6) in regard of the increasing acceleration signal. Moreover, the multiplying factor between one- and two-story is 2.1, 2.0, and 2.3 for the three signals. These indicate the limited impact on the ridge displacement of the second story in regard of the impact discussed before on the shear wall.

An additional impact comes from the inertial effect of the concrete slab (because of a mass increase of 29%). Figure 18 takes into account this mass. However, this increases the drift of the first story in the shear wall only about 17% comparing simulations 1–1a and about 9% comparing simulation 3–3a. Then the impact of the



(a) 100% signal, one-storey house (simulation 1-os)

(b) 100% signal, two-storey house (simulation 1)

(c) 200% signal, one-storey house (simulation 2-os)

(d) 200% signal, two-storey house (simulation 2)

(e) 300% signal, one-storey house (simulation 3-os)

(f) 300% signal, two-storey house (simulation 3)

Figure 16. Deformed configuration (amplification factor: 50) for an acceleration in y-direction, displacement in [mm].

mass of slab decreases as the signal amplitude increases. Figure 19 shows the displacement at the corner of the wall (nodes ⓐ,ⓑ, and ⓒ) for a 100% signal (simulations 1-os, 1 and 1a) and for a 300% signal (simulation 3-os, 3, and 3a). The second story itself leads to a much stronger increase for the displacements, whereas the mass of the slab has a minor influence. A reason for this is the different distribution of the mass; for the slab the whole mass is added at the ceiling level, the mass of the second story is distributed on a height of 2 m. Besides, the total added mass of the slab is 3000kg; the mass of the walls of one story is 5400 kg. Then, the impact of the mass slab is not a predominant factor in the dynamic behavior of the two-story house in regard to the response of the excitation of walls.

Acceleration in x-direction

As the y-direction shows, the mass of the slab has not an important impact then in the x-direction of acceleration it is assumed that the mass slab is not considered. The results for all acceleration signals in x-direction are shown in Table 4 and the deformed configuration are presented in Figure 20. For an acceleration in x-direction, the walls containing only

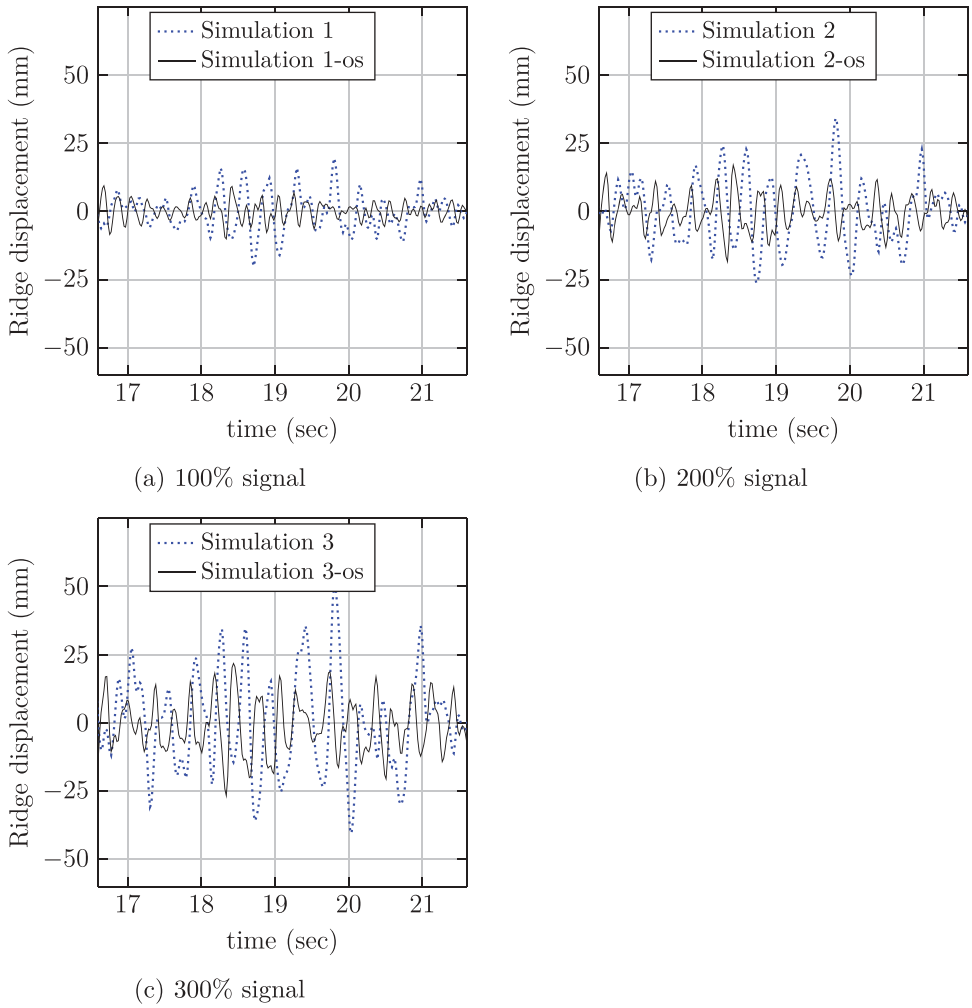
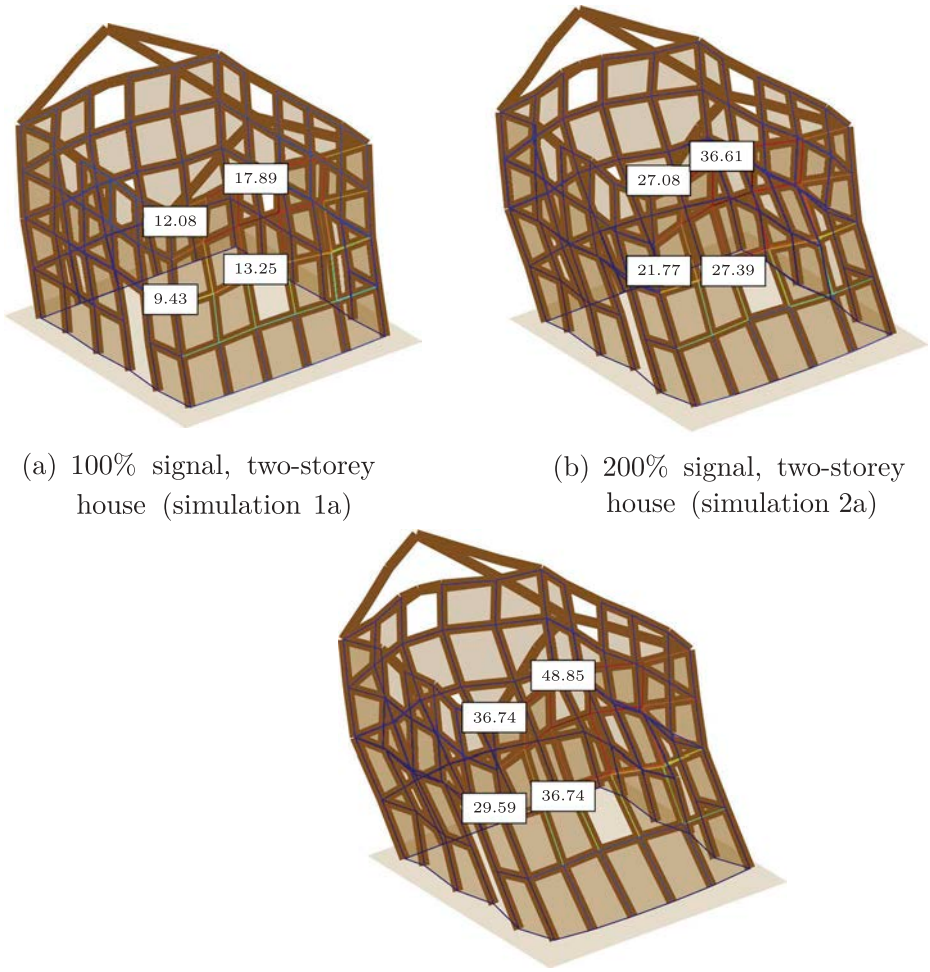


Figure 17. Ridge displacement in y-direction near the strong phase of the three signals.

two windows and no door function as very stiff shear walls. For the acceleration in *y*-direction however, each shear wall contains one door and two windows and is thus weaker. Moreover, the roof has a higher stiffness in *x*-direction and increases the resistance in this direction supporting the shear walls. Therefore, the drift of the two-story house in the first story of the shear wall decreases for the acceleration in *x*-direction from 0.375% (*y*-direction) to 0.21% (*x*-direction) for signal 100% and from 1.35% (*y*-direction) to 0.9% (*x*-direction) for signal 300%. In return, the drift of the weakener front wall has a limited increase from 1.93% to 2.00% for signal 300%. The Figure 21 shows that the *y*-loading acceleration give a predominant response of the shear wall excitation that *x*-loading direction. Due to the effect of the girders carrying the slab only in the *x*-direction, the displacement at the middle of the front wall is more pronounced for the solicitation in *x*-direction compared to the solicitation in *y*-direction. Note that the large deformation obtained in the middle of the horizontal beam is due to the unbraced girders.

Hysteretic behavior

To evaluate the hysteretic behavior, the temporal course of the drift of the first story and the second story for the two houses (one-story and two-story) in relation with the sum of the horizontal forces (i.e., global force) for an acceleration in *y*-direction is shown in Figures 22–24. The effective stiffness values are summarized in Table 5 and have been derived by computing the slope connecting the positive and negative peak base global forces and the corresponding displacement from the graphs in Figures 22–24. The hysteretic responses of structure is related with the nonlinearity and dissipated energy include in the model which lead to a decrease of the stiffness. For the one-story house (Figure 22), the overall behavior is linear for the ground motion equivalent to Haiti's

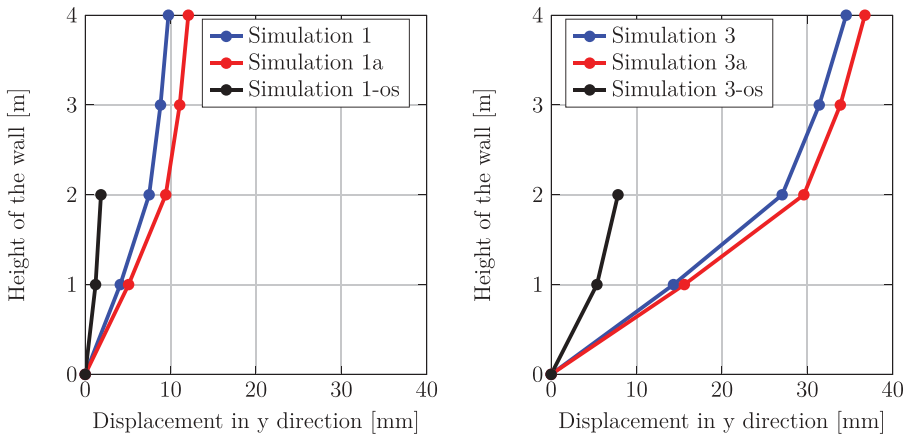


(a) 100% signal, two-storey house (simulation 1a)

(b) 200% signal, two-storey house (simulation 2a)

(c) 300% signal, two-storey house (simulation 3a)

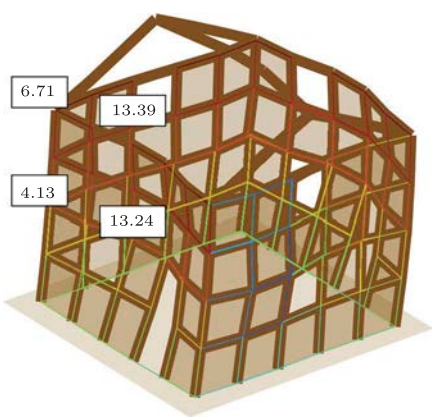
Figure 18. Deformed configuration (amplification factor: 50) for an acceleration in y-direction and an additional mass of the slab, displacement in [mm].



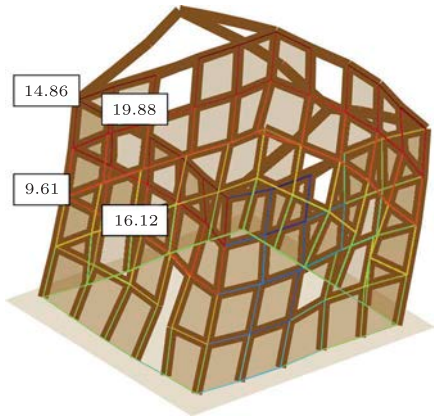
(a) 100% signal

(b) 300% signal

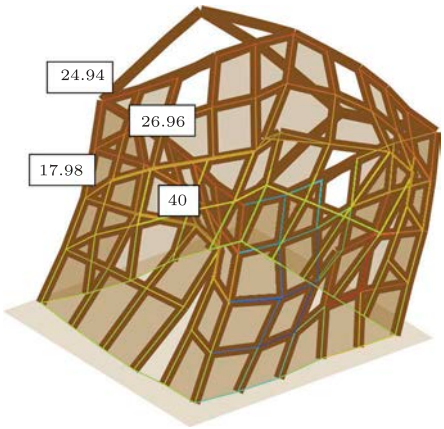
Figure 19. Displacement at the corner of the shear wall (nodes ⓐ,ⓑ, and ⓒ) for the one-story and two-story house (acceleration in y-direction).



(a) 100% signal, two-storey house (simulation 1x)

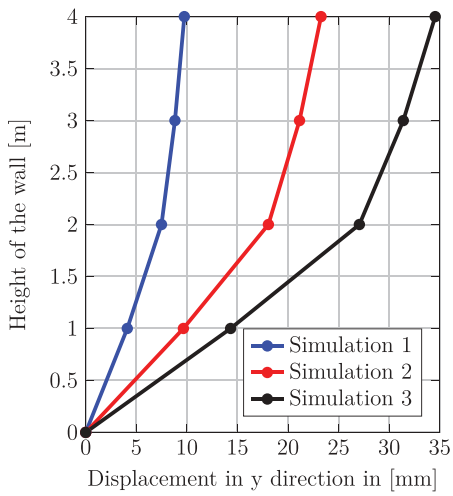


(b) 200% signal, two-storey house (simulation 2x)

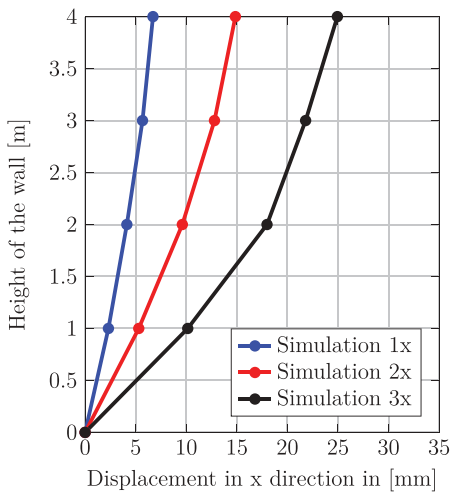


(c) 300% signal, two-storey house (simulation 3x)

Figure 20. Deformed configuration (amplification factor: 50) for an acceleration in x-direction, displacement in [mm].

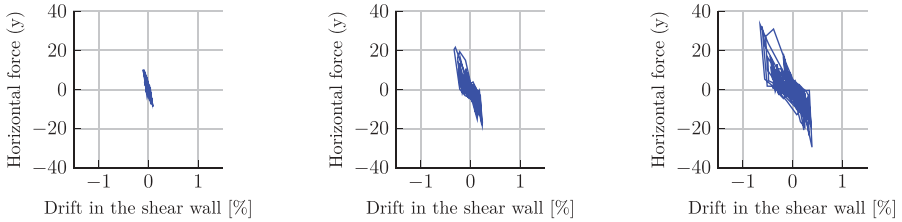


(a) Two-storey house (acceleration in y-direction)



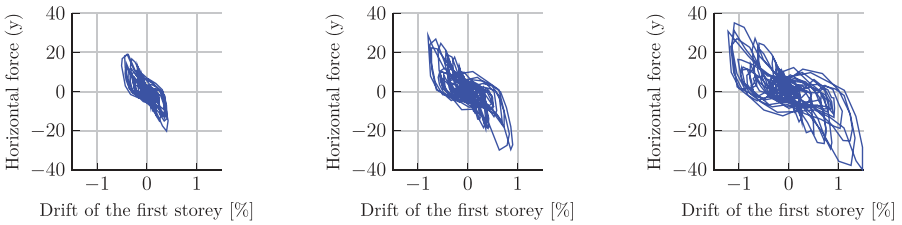
(b) Two-storey house (acceleration in x-direction)

Figure 21. Displacement at the corner of the shear wall.



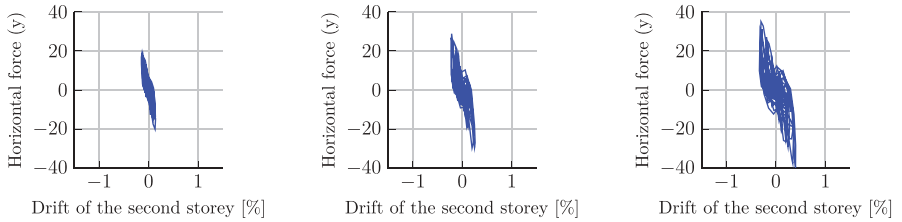
(a) 100% signal (simulation 1-os) (b) 200% signal (simulation 2-os) (c) 300% signal (simulation 3-os)

Figure 22. Global horizontal force vs. drift (one-story house) in shear wall (y-direction).



(a) 100% signal (simulation 1) (b) 200% signal (simulation 2) (c) 300% signal (simulation 3)

Figure 23. Global horizontal force vs. drift of the first story (two-story house) in shear wall (y-direction).



(a) 100% signal (simulation 1) (b) 200% signal (simulation 2) (c) 300% signal (simulation 3)

Figure 24. Global horizontal force vs. drift of the second story in shear wall (y-direction).

Table 5. Effective stiffness (y-direction).

Signal	One-story	First story	Second story	Unit
Haiti 100%	4.76	2.47	7.45	[KN/mm]
Haiti 200%	3.69	2.04	7.10	[KN/mm]
Decrease ratio (Haiti 100%)	−23	−17	−5	[%]
Haiti 300%	3.00	1.45	5.36	[KN/mm]
Decrease ratio (Haiti 100%)	−37	−41	−28	[%]

January 2010 earthquake (acceleration at 100%). Then, the nonlinearity increase for the acceleration signal of 200% and 300% but in a limited extent. The effective stiffness decrease in a most significant way, from −23% to −37% with the signal of Haiti 200% and 300%. For the two-story house, the first story (Figure 23) exhibits for all signals an inelastic behavior which increases at each signals. This reveals structural damage. The effective stiffeness deacrese in the same proportion of the one-story house. For the second story, the nonlinearity behavior are not so clear for the signal 100% and very limited for the others, in a same way of the one-story house. This is also obtained with the effective stiffness. Then, structural damage is very low compared to the first story. This finding can be explained by the position of the center of the gravity which is a the slab level, as the roof mass is very low and neglected in the model.

Discussion

This discussion about the failure mode focuses on the uplift at the steel strip which is undeniably the key-issues of this work. Over failure modes, not investigate in this study, are also possible such as the infill falling. To

evaluate the resistance of the timber-framed structure, a failure criterion must be determined. For the house, the steel strip supports at the bottom of the house are supposed to be the controlling element for the failure of the structure. This connection resists to a high compression but will fail under tensile stress. The maximum tensile stress due to the horizontal seismic load is imposed onto the bottom supports at the corners of a shear wall (node ⓐ). Consequently, this maximum tensile force during the dynamic loading is compared to the maximum tensile resistance of a static tensile test for the connection. The relation between the tensile force and the vertical displacement for the connection with eight nails according to static tests in Vieux-Champagne (2013) is shown in Figure 26. The maximum tensile force was identified with 11 kN, which is equivalent to a vertical displacement of 11 mm. To respect a certain safety, the static maximum potential tensile force must be reduced to get a maximum permitted tensile force. A reference value for this force can be found via a maximum permitted drift of a story. According to on Eurocode 8, the damage limitation state (serviceability seismic action), for buildings having non-structural elements not interfering with the structure, is: $d_r v < 0.01h$. d_r is the interstory drift, h is the story height, v is the reduction factor that is dependent on the level of significance of the structure (to simplify, it is supposed here that $v = 1$). The damage limitation expressed in terms of drift d_r is used to derive an equivalent ultimate limite state associated with the connections. For the both houses (one- and two-story), the relation between the drift and the vertical displacement for a static horizontal force is simulated. The load is applied in the same way at the top of the two shear walls. Due to the lower impact on the structure of the loading acceleration in x-direction, only the resistance in the y-direction is investigated . As shown in Figure 25, the drift limit of 1% corresponds, respectively, for one-story and two-story house of 2.65 mm and 3.64 mm of vertical displacement of bottom

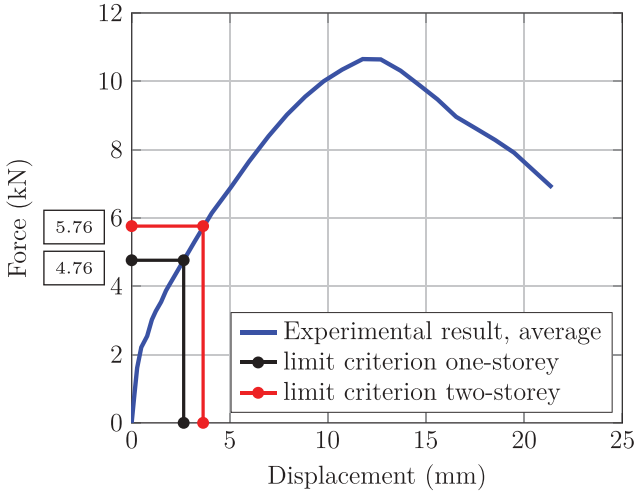


Figure 26. Steel strip connection under tensile loading (experimental data from Vieux-Champagne (2013)).

strip metal. These values lead to a tensile force of 4.76 kN for the one-story house and 5.76 kN for the two-story house (Figure 26).

A maximum permitted tensile force equal to 52% of the maximum static potential force of the steel strip has been reached in the connections. If one compares the results in Tables 3 and 4 with this limit force, one can see the following.

- The one-story house resists for all seismic signals, as the tensile force in the steel strip is never higher that the limit criterion (4.76 kN). This results are correlated by the experimental work with shake table test presented in Vieux-Champagne et al. (2017) and Sieffert et al. (2016). No damage has been observed at these level of earthquake signals in shear walls.
- The two-story house with a light-weight slab or with a thin concrete slab also resists for the 100% acceleration signal. The maximum value of the

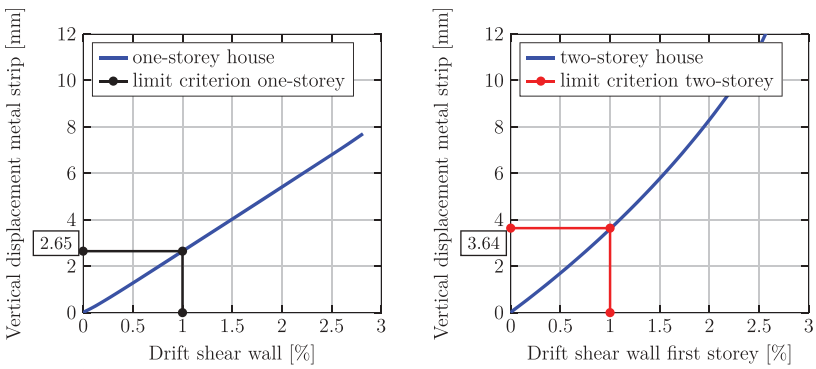


Figure 25. Drift of the first story shear wall vs. vertical displacement of the bottom steel strip for static loading (in y-direction).

tensile force in the steel strip is lower than the limit criterion (5.76 kN). This gives the proof of the seismic-resistant behavior of a filled timber-framed structure with two-story based on the damage limitation requirement of the Eurocode 8 §4.4.3. At an increased seismic level (200% and 300% signal), the tensile force in the steel strip exceeds the limit criterion. Let's note that with these signals, the tensile force in the steel strip are still lower that the maximum experimental value (11 kN). The maximum tensile force in the steel strip is obtained for the thin concrete slab and 300% signal and it equates to 68% of the maximum static potential force. Then the two-story house should be not collapsed even at this high level of ground motion signal.

Conclusion

This article has presented a numerical analysis for two-story timber-framed structures. One of the main advantages of the numerical model developed was also highlighted: the possibility to take into account nonlinear and hysteresis behavior with a simple model which needs only 734 degrees of freedom for a two-story house. It is assumed that the nonlinear behavior of the structure was concentrated in specific components of the building. Then, seismic loading was applied with the use of an synthetic signal of the Haiti earthquake from January 12, 2010. Next, the signal was increase by a factor two and three (200% and 300%) so as to analyze the nonlinear structural behavior. Two kinds of building were simulated and compared: one- and two-story building. Two directions of acceleration loading was also investigated. The view of deformed configuration has revealed the predominance of the wall masses compared with the slab mass and also of the y-direction of loading in regards to x-direction for the two-story house. Special attention was paid to quantify the hysteresis behavior of the one- and two-story. For the 100% signal, in accord with previous experimental works, the one-story house was stayed in elastic behavior, while the two-story house displays non-linearities. The most important innovation in this paper is to develop a failure criterion to seismic-resistance quality and validates the relevance of this type of building in Haiti's reconstruction project after the earthquake of Port-au-Prince, January 12, 2010. This criterion is based on static loading which may be used easily by engineer who work in field. The tensile force, in steel strip connetions, obtained by seismic signal loading was compared with the criterion. For the Haiti 100%, scientific proof was made of the seismic-resistance quality of a filled timber-framed structure with one- or two-story. At an increase seismic level (200% and 300% signal), the response of the one-story house was also under the criterion, while the response of the two-story house was exceeded the limit. The article concluded that even in these high level of ground motion signal, the two-story house should not be collapsed and then should be promoted for reconstruction project.

Acknowledgments

The authors would like to thank and acknowledge the French National Research Agency (ANR) for its support of the "ReparH" project, under reference code ANR-10-HAI-003 (as coordinated by CRAterre in collaboration with UJF-3SR, the AE&CC Research Unit of ENSAG and the Haitian NGO GADRU), along with all participating associations of the PADED platform and local partners for their involvement and contributions to this endeavor.

This work has been realized in the framework of the VOR program of Univ. Grenoble-Alpes, the LABEX AE&CC and the IDEX CDP Risk@Univ. Grenoble Alpes as part of the program "Investissements d'Avenir" overseen by the French National Research Agency (reference: ANR-15-IDEX-02). The authors extend their gratitude to and acknowledge to Julien Hosta for his help in the definition of the two-story house model.

ORCID

Y. Sieffert http://orcid.org/0000-0002-6971-7857
S. Grange http://orcid.org/0000-0002-7766-0483

References

Andreasson, S., M. Yasumura, and L. Daudeville. 2002. Sensitivity study of the finite element model for wood-framed shear walls. *Journal of Wood Science* 48(3):171–78. doi:10.1007/BF00771363.

Boudaud, C., J. Humbert, J. Baroth, S. Hameury, and L. Daudeville. 2015. Joints and wood shear walls modelling II: Experimental tests and fe models under seismic loading. *Engineering Structures* 101:743–49. doi:10.1016/j.engstruct.2014.10.053.

Dolan, J. 1989. The dynamic response of timber shear walls. Ph.D. thesis, University of British Columbia.

Dutu, A., H. Sakata, and Y. Yamazaki. 2014. Experimental study on timber-framed masonry structures. *Historical Earthquake-Resistant Timber Frames in the Mediterranean Area* 67–81. doi:10.1007/978-3-319-16187-7_6.

EN 338. 2003. Structural timber - Strength classes.

Grange, S. 2016. AtlAs—A tool and language for simplified structural solution strategy. Internal Report, GEOMAS INSA-Lyon, Villeurbanne, France.

Humbert, J. 2010. Characterization of the behavior of timber structures with metal fasteners undergoing seismic loadings. Ph. D. thesis, Grenoble University.

Humbert, J., C. Boudaud, J. Baroth, S. Hameury, and L. Daudeville. 2014. Joints and wood shear walls modelling I: Constitutive law, experimental tests and fe model under

quasi-static loading. *Engineering Structures* 65:52–61. doi:10.1016/j.engstruct.2014.01.047.

Joffroy, T., P. Garnier, A. Douline, and O. Moles. 2014. *Reconstruire Haïti après le séisme de janvier 2010: Réduction des risques, cultures constructives et développement local*. CRAterre. https://hal.archives-ouvertes.fr/hal-01159759.

Kasal, B., R. J. Leichti, and R. Y. Itani. 1994. Nonlinear finite-element model of complete light-frame wood structures. *Journal of Structural Engineering* 120(1):100–19. doi:10.1061/(ASCE)0733-9445(1994)120:1(100).

Kohrs-Sansorny, C., F. Courboulex, M. Bour, and A. Deschamps. 2005. A two-stage method for ground-motion simulation using stochastic summation of small earthquakes. *Bulletin of the Seismological Society of America* 95 (4):1387–400. doi:10.1785/0120040211.

Langenbach, R. 2007. From 'opus craticium' to the 'chicago frame': Earthquake resistant traditional construction. *International Journal of Architectural Heritage, Taylor & Francis* 1(1):29–59. doi:10.1080/15583050601125998.

Newmark, N. M. 1959. A method of computation for structural dynamics. *Journal of the Engineering Mechanics Division* 85(3):67–94.

Richard, N., L. Daudeville, H. Prion, and F. Lam. 2002. Timber shear walls with large openings: Experimental and numerical prediction of the structural behaviour. *Canadian Journal of Civil Engineering* 29(5):713–24. doi:10.1139/l02-050.

Ruggieri, N., G. Tampone, and R. Zinno. 2015. *Historical earthquake-resistant timber frames in the mediterranean area -, 2015th edition*. Berlin, Heidelberg: Springer.

Sieffert, Y., J.-M. Huygen, and D. Daudon. 2014. Sustainable construction with repurposed materials in the context of a civil engineeringearchitecture collaboration. *Journal of Cleaner Production* 67:125–38. doi:10.1016/j.jclepro.2013.12.018.

Sieffert, Y., F. Vieux-Champagne, S. Grange, P. Garnier, J. Duccini, and L. Daudeville. 2016. Full-field measurement with a digital image correlation analysis of a shake table test on a timber-framed structure filled with stones and earth. *Engineering Structures* 123:451–72. doi:10.1016/j.engstruct.2016.06.009.

Vieux-Champagne, F. 2013. Analyse de la vulnÃ©rabilitÃ© sismique des structures Ã ossature en bois avec remplissage. Ph.D. thesis, UniversitÃ© de Grenoble, Ecole Doctorale IngÃ©nierie IMEP 2, Laboratoire 3SR.

Vieux-Champagne, F., S. Grange, Y. Sieffert, P. Garcia, C. Faye, J.-C. Duccini, and L. Daudeville. 2014a. Numerical analysis of timber-frame structures with infill under seismic loading. World Conference on Timber Engineering (WCTE) 2014, Quebec City, Canada, August 10–14.

Vieux-Champagne, F., Y. Sieffert, S. Grange, C. Belinga Nko'o, E. Bertrand, J.-C. Duccini, C. Faye, and L. Daudeville. 2017. Experimental analysis of a shake table test of a timber-framed structures with stone and earth infill. *Earthquake Spectra* 33:1075–100. doi:10.1193/010516EQS002M.

Vieux-Champagne, F., Y. Sieffert, S. Grange, A. Polastri, A. Ceccotti, and L. Daudeville. 2014b. Experimental analysis of seismic resistance of timber-framed structures with stones and earth infill. *Engineering Structures* 69:102–15. doi:10.1016/j.engstruct.2014.02.020.

White, M. W., and J. D. Dolan. 1995. Nonlinear shear-wall analysis. *Journal of Structural Engineering* 121(11):1629–35. doi:10.1061/(ASCE)0733-9445(1995)121:11(1629).

Xu, J., and J. D. Dolan. 2009. Development of a wood-frame shear wall model in abaqus. *Journal of Structural Engineering* 135(8):977–84. doi:10.1061/(ASCE)ST.1943-541X.0000031.

Yasumura, M., T. Kamada, Y. Imura, M. Uesugi, and L. Daudeville. 2006. Pseudodynamic tests and earthquake response analysis of timber structures II. *Journal of Wood Science* 52(1):69–74. doi:10.1007/s10086-005-0729-4.

A. Mass of the slab

The slab consists of a bearing structure made out of wood and an insulation layer of hydraulically bound materials. For a general use, the mass of a slab consisting of the wooden bearing structure and a 7 cm screed layer is calculated. The weight of the girders (8 kg/m) is neglected. For a distance of 0.9 m between the girders and a length of 4.5 m of a girder, the load onto one girder is

$$m_{girder} = 2200\text{kg/m}^3 \cdot 0.9\text{m} \cdot 4.5\text{m} \cdot 0.07\text{m} = 623\text{kg}.$$

For the built house on Grand Boulage, a light hemp concrete is used for insulation:

$$\rho_{light} = 100\text{kg/m}^3$$

$$d = 15\text{cm}$$

$$m_{girder} = 100\text{kg/m}^3 \cdot 0.9\text{m} \cdot 4.5\text{m} \cdot 0.15\text{m} = 61\text{kg}.$$

The mass of this slab is relatively small compared to the mass of one cell of the wall (150 kg).

B. Natural frequencies of the houses

Table B.1. Natural frequencies for the one-story and the two-story house.

	one-story house	two-story house	two stories house with concrete slab
f_1 [Hz]	5.2	3.3	2.3
f_2 [Hz]	5.3	3.7	3.5

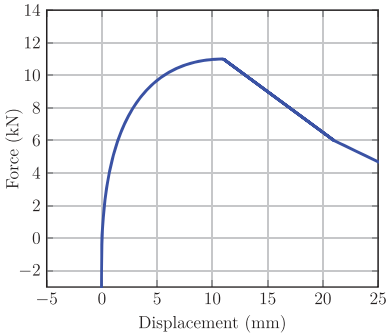
C. Parameter values Humbert element

Table C.1. Model parameters governing the constitutive behavior under monotonic loading.

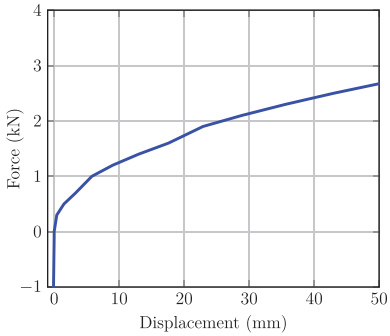
	Value					
	Diagonal X-crosses		Steel Strip			
Parameters	Tension	Compression	Shear	Tension	Compression	Unit
d_y	.005	0.002	0.9	0.1	0.005	mm
d_1	3500	415	48	11	0.5	mm
d_2	3750	425	65	21	20	mm
d_u	4000	450	90	39	25	mm
F_1	12	48.6	17.25	11	39	kN
F_2	2.5	45	12.18	6	20	kN
F_u	1	40	2.03	0.1	0.1	kN
K_0	3.86	42	2.48	10	80	kN/mm
K_1	0	0	0	0.4	0	kN/mm

Table C.2. Model parameters governing the constitutive behavior under cyclic loading.

	Value					
	Diagonal X-crosses		Steel Strip			
Parameters	Tension	Compression	Shear	Tension	Compression	Unit
C_1	−1	−2	.1	−1	−2	-
C_2	−0.5	−1	.1	−0.5	−1	-
C_3	0.01	.1	.2	.01	.1	-
C_4	0.9	0.5	.75	0.9	0.5	-



(a) Steel strip connection



(b) Diagonal X-crosses

D. Wooden skeleton

Table D.1. Dimensions of structural members.

Member	Dimensions (mm^2)
Corner column	100 × 100
Vertical interior colums	50 × 100
Horizontal beams	100 × 50
Floor girders	2 × (50 × 200)
Ridge beam	50 × 50
Common purlin	50 × 50
Diaphram diagonal beams	50 × 100
Horizontal mid-height bars	27 × 100

Table D.2. Mechanical properties (class C18, [EN~338(2003)]).

Parameter	Symbol	Value	Unit
Young modulus	E	9000	MPa
Shear modulus	G	560	MPa
Density	ρ	390	Kg/m^3